

Computational Laboratory 2

Pierre Fritz, Lorenzo Filippi, Andrea Capuano, Gabriele Lecce, Simone Radaelli

May 8, 2025

1 Introduction and simulation parameters

In this computational laboratory, we have performed several simulations using the Smilei 2D Particle-In-Cell code. In Question 1 simulations have been performed varying the normalized laser intensity parameter a_0 at a fixed plasma density $n_0 = 0.1n_c$, while in Question 2 the plasma density was varied at a fixed $a_0 = 10$. The setup parameters provided in the script "input.py" have been modified in order to get reliable simulation results and avoid non-physical behaviours of the laser-plasma interaction.

The spatial discretization of the domain ($\Delta x = 15\text{ppm}$, $\Delta y = 15\text{ppm}$) has been lowered to reach a compromise between resolving correctly the Debye length of the plasma ($\lambda_D > \Delta x, \Delta y$) and having a manageable simulation time. The number of macroparticles per cell has been set "high enough" ($nppc_{ion} = 10$, $nppc_{ele} = 10$) after some trial simulations, although lower values of $nppc_{ion}$ may also be fine because the laser is mainly interacting with the electronic population. Moreover, an aftertarget zone of $20\mu\text{m}$ has been added to observe the physical behaviour of the laser-plasma interaction after the laser exits the plasma.

```
# BOX PARAMETERS
target_thickness = 100 * um # Thickness of the target
targetstart = 20 * um # Start position of the target
aftertarget = 20 * um # Distance after the target
Lx = targetstart + target_thickness + aftertarget # Total length of the box along x-axis
Ly = 40 * um # Total length of the box along y-axis
resx = 15 # Points per micron in x-direction, ho cambiato da 10 a 15
resy = 15 # Points per micron in y-direction

# PLASMA PARAMETERS
Temp = 0.2 / mc2 # Temperature of the plasma in eV
Z_H = 1 # Charge number of the ions (Carbon)
A_H = 1 # Atomic mass number of the ions (Carbon)
species_boundary_conditions = [['remove'], ['periodic']] # Boundary conditions for species
n_target = 0.1 # Number density of the target in units of critical density
nppc_ion = 10 # Number of ions per cell
nppc_ele = 10 # Number of electrons per cell
```

Figure 1: Main box parameters of the simulation. The modified "input.py" and the results of the simulations have also been uploaded in the project Github repository. [1].

The simulated laser has a pulse duration of 23fs in the range of intensities $a_0 = 0.1 \div 50 \rightarrow I = (0.02 \div 5400) \cdot [10^{18} \cdot W/cm^2]$ at the vacuum wavelength $\lambda_0 = 800\text{nm}$.

2 Question 1

The simulation implements a laser with a normalized laser intensity parameter defined as:

$$a_0 = \frac{eE_0}{m_e\omega c} \quad (1)$$

where e is the electron charge, E_0 is the peak electric field amplitude, m_e is the electron mass, ω is the laser angular frequency and c is the speed of light. Four simulations are performed with intensity

values of $a_0 = 0.1, 1, 10, 50$ at a fixed $n_0 = 0.1n_c$, where n_c the critical density of the plasma, defined as:

$$n_c = \frac{\varepsilon_0 \gamma m_e \omega^2}{e^2} \quad (2)$$

where ε_0 is the vacuum permittivity, $\gamma = \sqrt{1 + a_0^2}$ is the average Lorentz factor of the plasma electrons (circular polarization), m_e is the electron mass, ω is the laser frequency, and e is the electron charge. It is possible to obtain the evolution of electrons total energy as a function of time for various values of a_0 (the density being fixed at $n = 0.1n_c$). The simulation results are plotted in the following graphs:

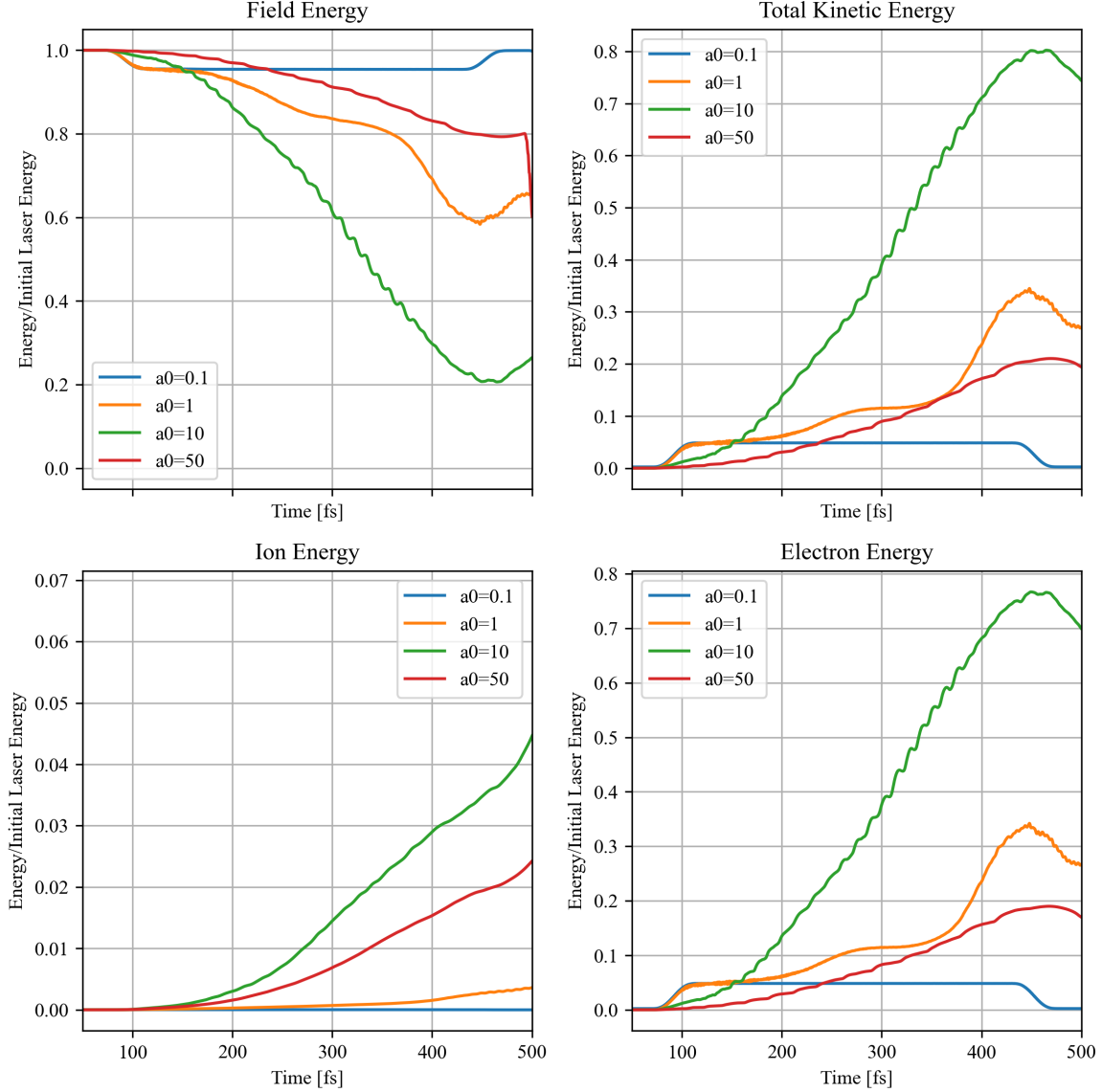


Figure 2: The plot shows different laser intensities ($a_0 = 0.1, 1, 10, 50$) over a time interval of $50 \div 500 \text{ fs}$.

The results are showed starting from the time instant 50 fs , so as to have the full laser pulse in the box. The energies shown in the plot have been normalized using a "Initial Laser Energy" which is the maximum intensity that the laser pulse have before interacting with the plasma.

As seen from the provided plots, the curve for $a_0 = 10$ displays the biggest drop in field energy. In

comparison, the other curves show a smaller drop, meaning a smaller absorption of energy from the plasma.

Now we analyze what happens for $a_0 = 10$, providing to snapshots of the relative simulation.

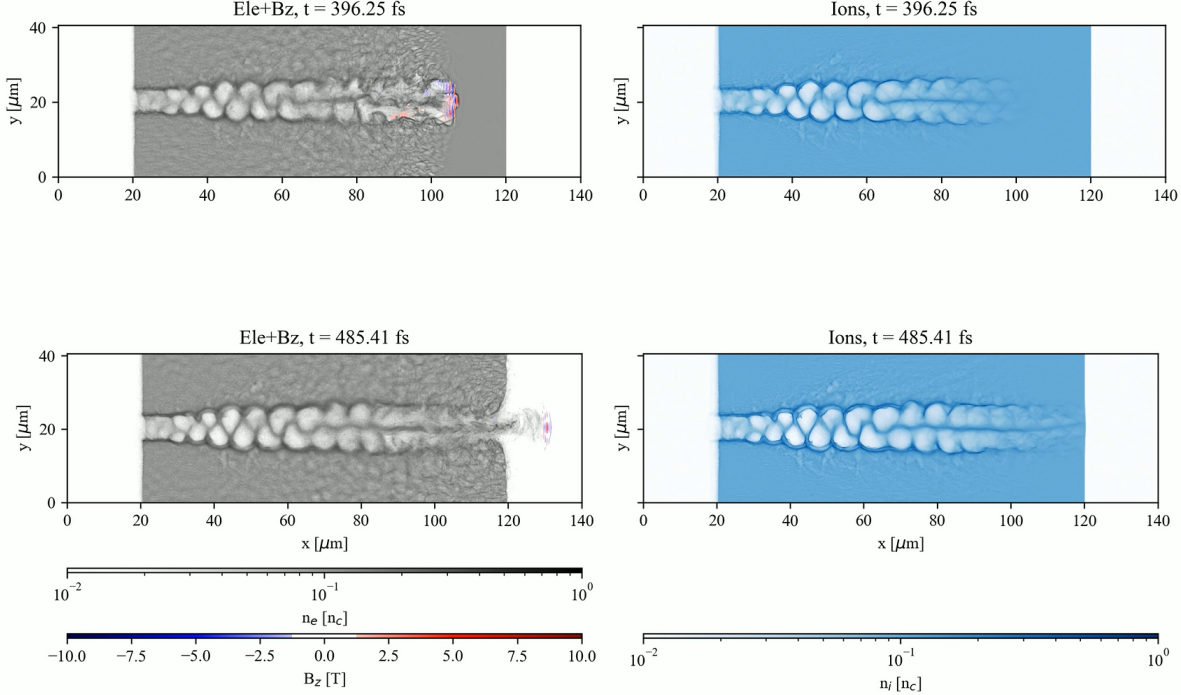


Figure 3: Densities and magnetic field of the laser-plasma interaction ($a_0 = 10$, $n_0 = 0.1$). Video.

In the upper part, it can be seen that at simulated time 396 fs the laser is traveling in the plasma, followed by a wakefield (which will be explained later in this report), while at simulated time 485 fs the laser exits the plasma with most of its energy depleted.

The simulation suggest strong direct laser acceleration (DLA) as the main transfer of energies between laser and plasma. In fact the strong intensity pulse create a plasma channel in which the transverse electric field of the laser accelerates the electrons that are in presence of a self generated longitudinal magnetic field, so the transverse momentum is converted into a longitudinal one, resulting into a resonance condition favorable for the direct absorption of energy to the electrons.

A secondary phenomena that can aid the absorption is the wakefield acceleration (WFA) where electrons are effectively "riding" the wake created by the laser. This phenomena "trap" the electrons in the plasma wake such that the laser phase velocity and electron motion match, allowing for strong coupling of the two and a favorable configuration for DLA.

To make a comparison with the other simulated intensity, we can see that at $a_0 = 50$ the absorption of energy is lower, with a decrease in field energy not as sharp, suggesting more complex behaviour due to different phenomena, like relativistic transparency onset. Also radiation pressure may push the plasma forward, reflecting part of the laser hence reducing absorption.

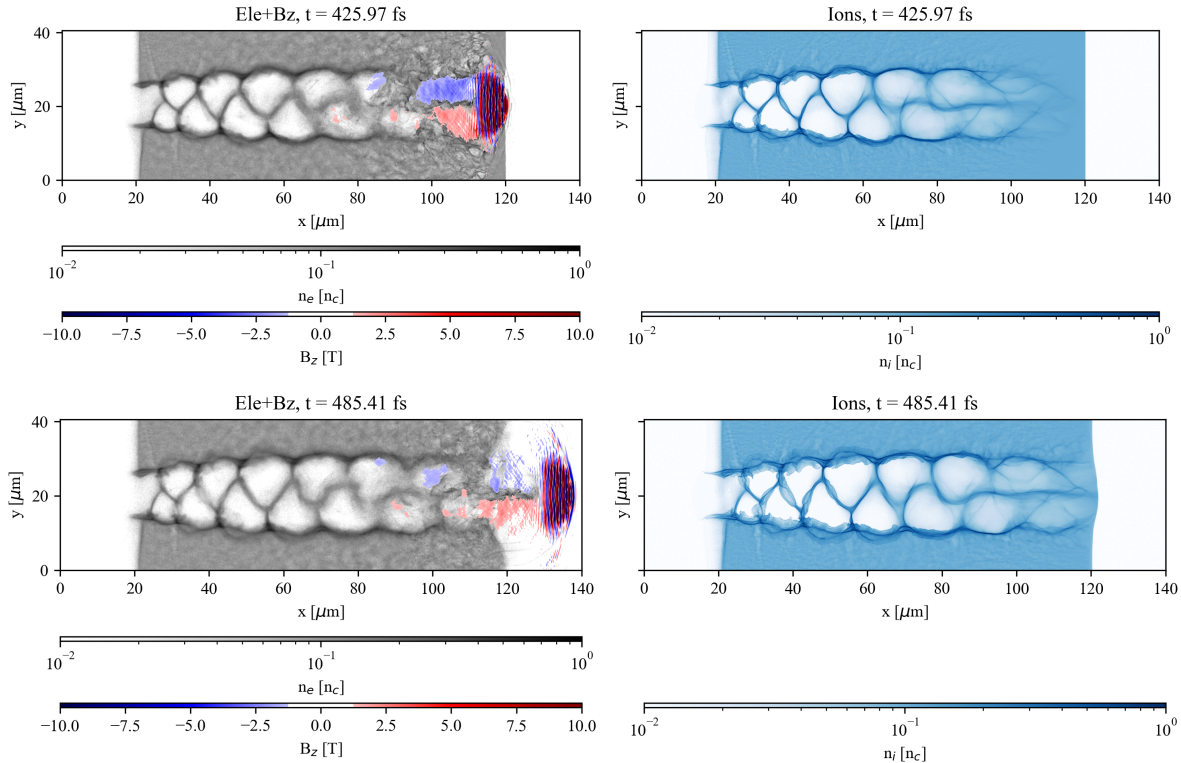


Figure 4: Densities and magnetic field of the laser-plasma interaction ($a_0 = 50$, $n_0 = 0.1$). Video.

In this snapshot (485fs) we can see a mature stage of the interaction between the plasma and the laser at $a_0 = 50$. The plot shows the a bubble-like structures in the underdense channel, typical of relativistic electron cavitation caused by the laser's ponderomotive force. Inside the structure we have a reduced density, confirming the presence of relativistic transparency that allow the pulse to go through the plasma.

Looking at the ion density we see that their motion tracks the bubble structure since they are pulled into the evacuated regions due to electrostatic fields left by expelled electrons. Their acceleration is also consistent with the ponderomotive force generated by the laser-plasma interaction.

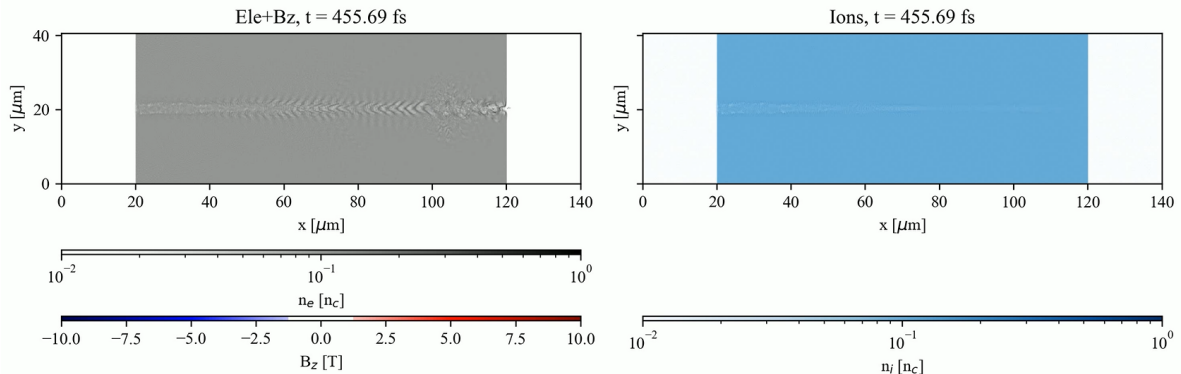


Figure 5: Densities and magnetic field of the laser-plasma interaction ($a_0 = 1$, $n_0 = 0.1$). Video.

With the snapshot of Figure 5, we can see that the laser is only weakly absorbed in the plasma, resulting in linear interaction regime with limited plasma heating.

In all the simulations, at around 450fs , the laser exits the plasma boundary, and it is possible to observe from the total kinetic energy that some of the energy of the electrons is transferred back to the field. This phenomena is overlapping with the drop of energy caused by the electrons exiting the boundary of the 2D box in the x-direction ("remove" boundary condition) and with the thermal transfer of energy to ions. Furthermore, from the "Ion Energy" plot, it is possible to observe that the ion population has no energy drop. Qualitatively this can be explained by saying that the ions don't interact much with the field due to their inertia, and the energy that is gained is mostly given by the electronic population. Moreover, the ion energy is moving slower than the electronic population (as shown in the density plots in the next paragraphs), so there is no energy drop due to the ions leaving the boundary of the box from the x-direction. In all the simulations it can be observed that the electronic population is interacting more with the laser, gaining an average energy of approximately one order of magnitude greater than the ion energy (e.g. for $a_0 = 10$, $E_{ele} \simeq 0.75E_{0,L}$, $E_{ion} \simeq 0.045E_{0,L}$).

It is to be highlighted that for the case $a_0 = 0.1$ there is a complete transfer of energy from the electron population to the laser, which, naively, seems to be a non-physical behaviour of the simulation which requires further examination of the theory or more simulations to be properly assessed. Regarding the densities and fields involved, during the laser passage through the plasma, laser wakefield acceleration occurs. The strong laser E field accelerates electrons in the opposite direction, while ions remain in their position, thus leading to charge separation and the formation of a restoring Coulomb force, so that electron density has oscillations proportional to plasma frequency. The electron experiences a strong attractive force toward the center of the plasma wave, and can become trapped. These are then further accelerated in the longitudinal direction as a result of the strong electric field generated by the charge separation.

So, the trapped electron can "ride" the plasma wave and can be accelerated up to relativistic energy in the pulse direction. acceleration continues until a large number of electrons reaches velocity comparable to the phase velocity of the plasma. Here, wave-breaking occurs with electrons being ejected at high speed.

3 Question 2

Another set of simulations are performed at fixed $a_0 = 10$ changing the density n_0 of the plasma target. For $a_0 \gg 1$ relativistic effects largely affects the laser-plasma interaction. The Lorentz factor γ affects for example the inertia of the electrons, which are not as quick as in non-relativistic regime in following the external fields. The simulation results are shown in the following graphs:

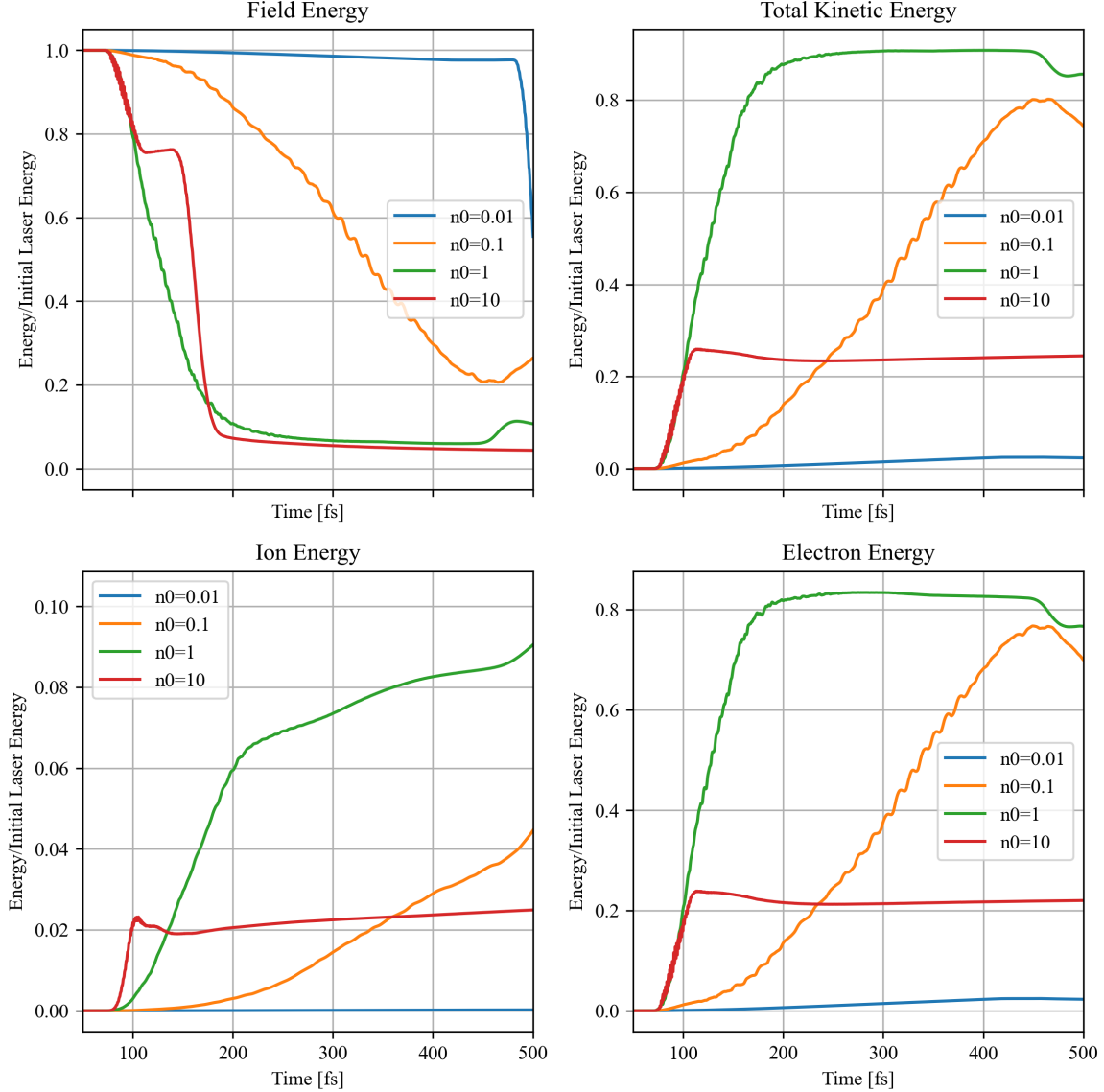


Figure 6: The plot shows different plasma densities ($n_0 = 0.01n_c, 0.1n_c, n_c, 10n_c$) over a time interval of $50 \div 500\text{ fs}$.

The maximum laser absorption occurs when the plasma density is equal to the critical density $n_0 = n_c$. At this condition, plasma and laser frequency are the same, enabling resonant coupling and efficient energy transfer from the laser to the plasma electrons. We can observe the behaviour of the laser-plasma interaction in the snapshots of Figure 7: in the first snapshot ($t = 99\text{ fs}$), the pulse enters the plasma and it begins to self-focus. At 128.78 fs the pulse keeps exchanging energy with the plasma, leaving a magnetization in the channel due to strong currents[3]. In the third snapshot (307.10 fs) most of the pulse energy has been transferred to the plasma and it is possible to observe the path of the pulse from the electrons density difference in the box.

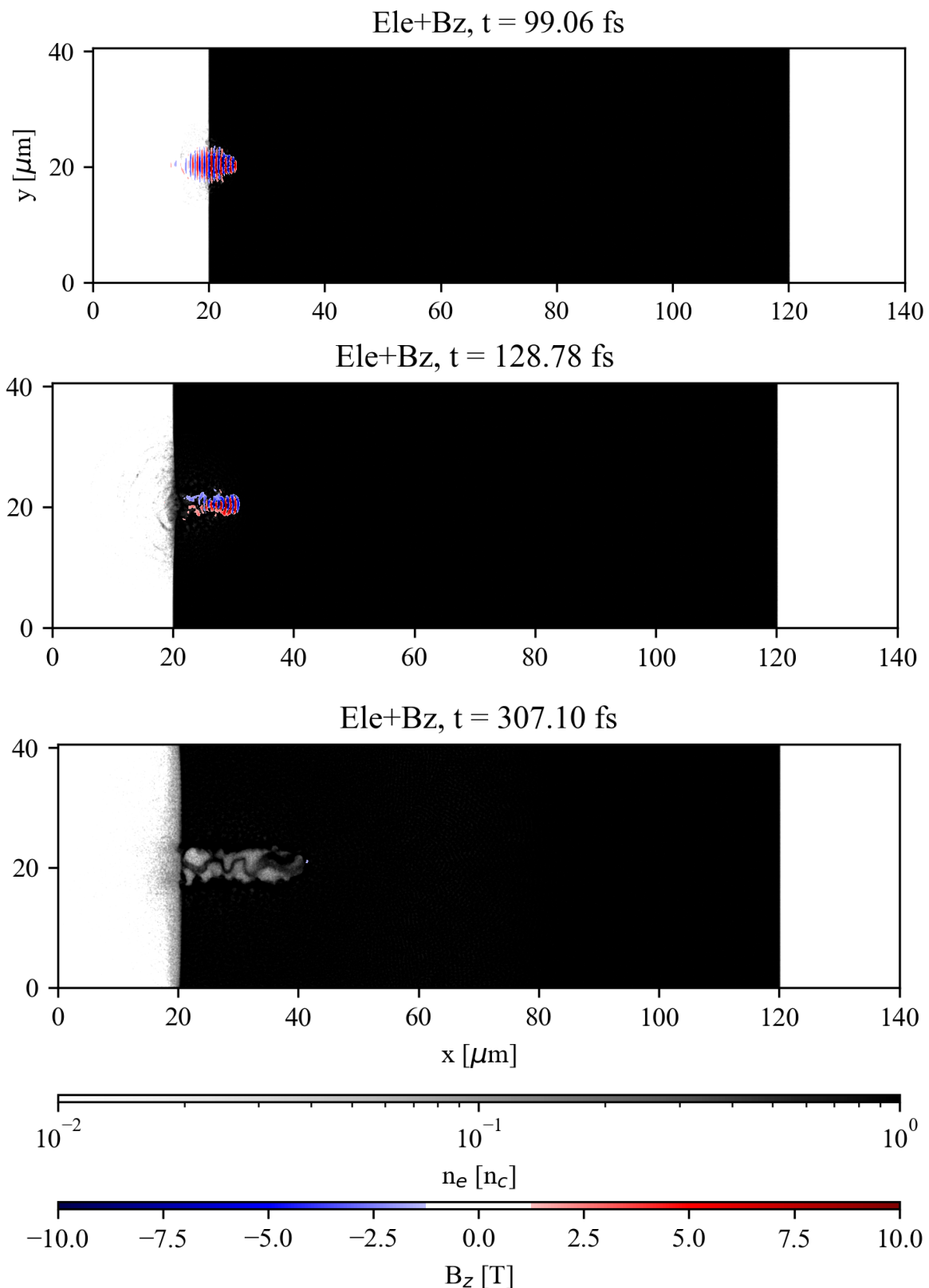


Figure 7: Densities and magnetic field of the laser-plasma interaction ($a_0 = 10$, $n_0 = 1$). Video.

For the underdense cases ($n_0 = 0.01n_c$ and $n_0 = 0.1n_c$), the laser pulse can propagate freely with minimal interaction, leading to a slower absorption. It is also possible to observe the channel formation

in this case, which with a combination of relativistic self-focusing and initial instabilities of the plasma seem to create a bifurcation as the pulse is propagating:

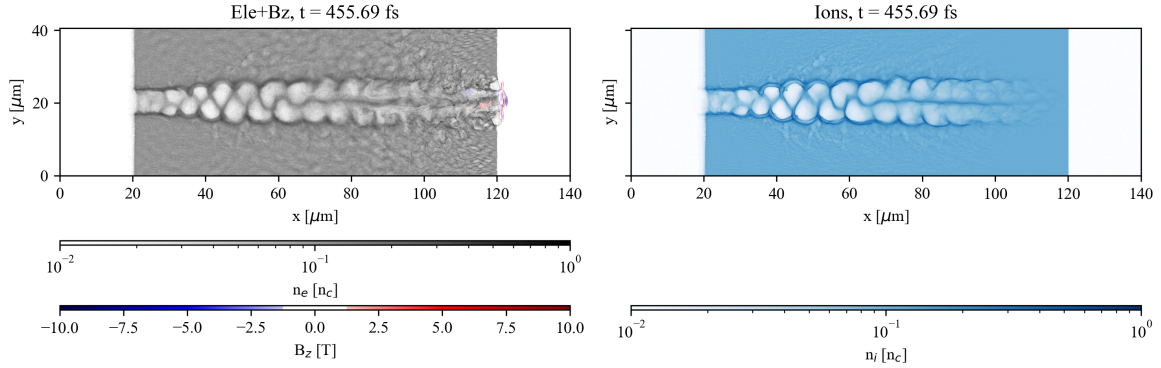
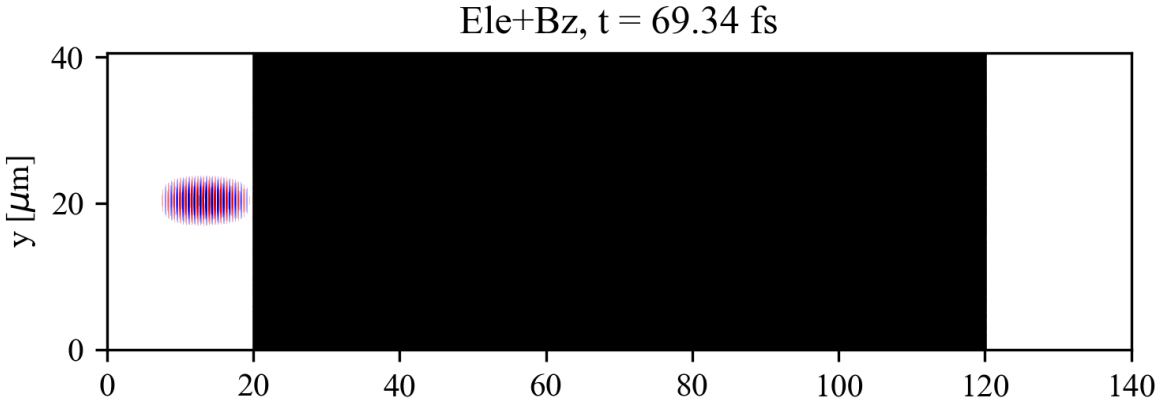


Figure 8: Densities and magnetic field of the laser-plasma interaction ($a_0 = 10$, $n_0 = 0.1$). The channel seems to bifurcate into two waveguides at around $60\mu\text{m}$. Video.

In contrast, in the overdense regime ($n_0 = 10n_c$), the laser is mostly reflected and attenuated at the plasma boundary ($x = 20\mu\text{m}, t \simeq 100\text{fs}$), and thus cannot deposit much energy in the plasma, resulting in reduced absorption ($E_{ele} \simeq 0.2E_{0,L}$, $E_{ion} \simeq 0.02E_{0,L}$). The reflection of the laser in the plasma can be qualitatively observed from the "Field Energy" plot at around 150fs , when there is an energy absorption due to the pulse exiting the boundary at $0\mu\text{m}$ (Silver-Muller boundary conditions). To summarize, both underdense and overdense conditions lead to reduced energy deposition due to ineffective coupling or strong reflection, respectively.



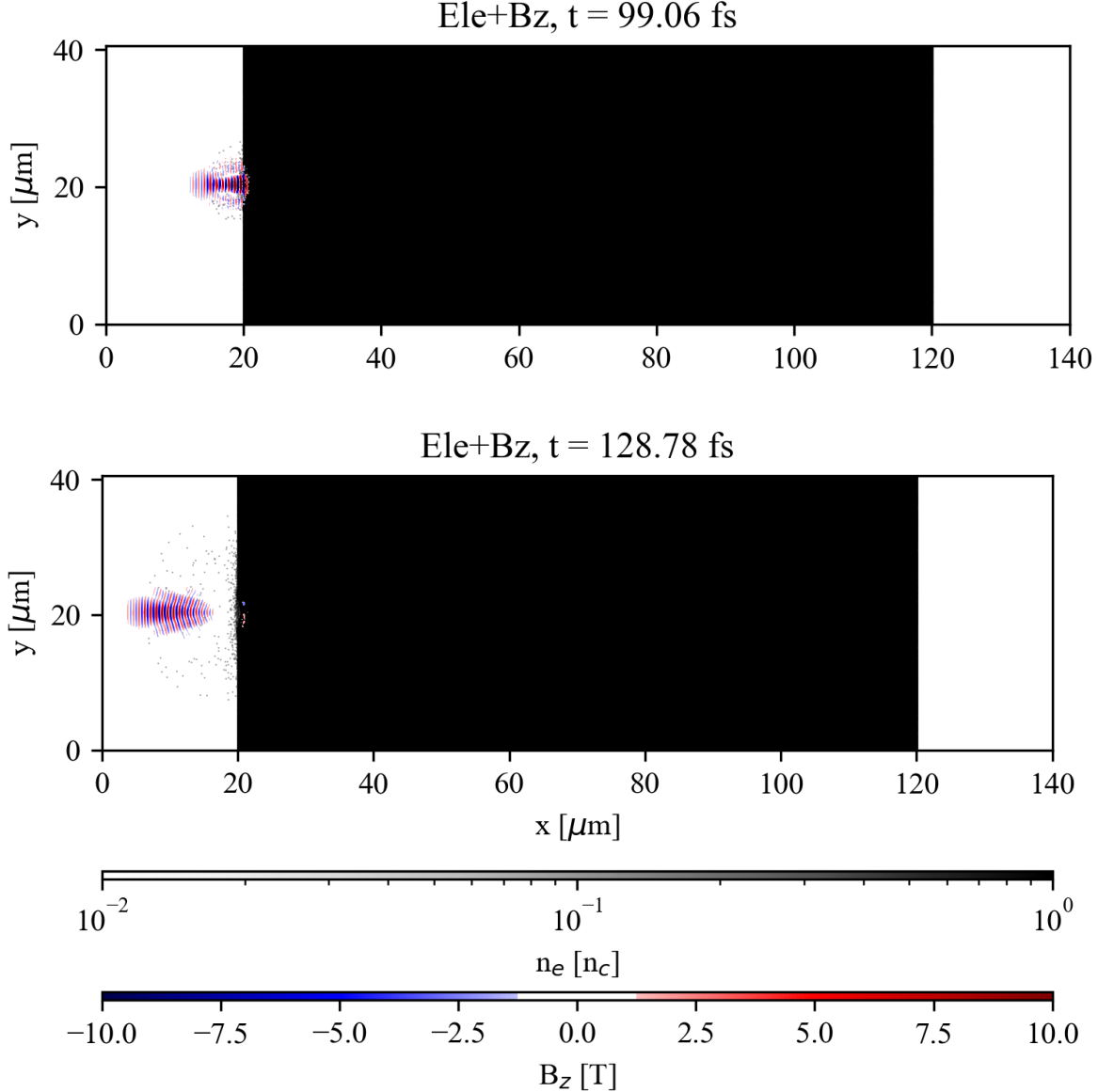


Figure 9: Densities and magnetic field of the laser-plasma interaction ($a_0 = 10$, $n_0 = 10$). The three snapshots show the reflection at the plasma boundary. Video.

The temperature of the plasma at the beginning of the simulation is set at $T = 0.2\text{eV}$. In order to estimate the temperature at a fixed instant, we retrieve from "plot_spectrum_electron.py" and "plot_spectrum_ion.py" the spectra of the electron and ion species at a fixed time $t \sim 300\text{fs}$, and fit each spectrum with a Maxwell-Boltzmann distribution function:

$$\frac{dN}{dE} = N_0 e^{-E/T}$$

We're using a MB distribution because we're interested in qualitative observations rather than quantitative, but it is important to notice that in many cases a MB distribution is different from the actual density function of the plasma species.[4]

To simplify the fit, we take the logarithm of the distribution function and get a linear expression:

$$\log\left(\frac{dN}{dE}\right) = y = \log(N_0) - \frac{E}{T} = A - \frac{E}{T}$$

Using the MATLAB toolbox "Curve Fitter" we perform the linear fit:

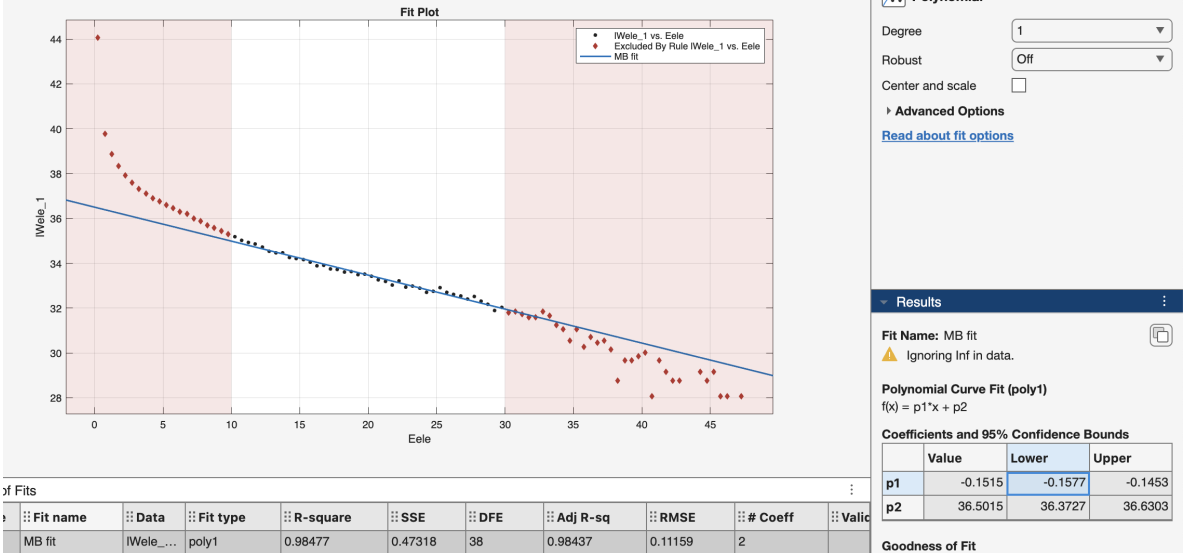


Figure 10: Linear fit for $a = 10$ and $n_0 = 0.1n_c$. We restrict the domain to $10 \div 30\text{MeV}$ to have more reliable results.

We fit the spectra of the simulations at $a_0 = 10$ and n_0 variable, obtaining the following results:

a_0	$n_0 [n_c]$	$T_{ele} [\text{MeV}]$	$T_{ion} [\text{MeV}]$
10	0.1	3.7 ± 0.3	0.12 ± 0.03
10	1	6.61 ± 0.26	0.75 ± 0.07
10	10	2.21 ± 0.58	0.56 ± 0.09

Table 1: Results of the Matlab fit for $a_0 = 10$ and n_0 variable.

The results obtained in Table 1, are consistent with the "Ion Energy" and "Electron Energy" plots of Figure 6: at $t \sim 300fs$, the energy of the electron and ion population is highest for the $n_0 = 1$ simulation. Indeed, for this value of density we also get the highest T_{ele} and T_{ion} . For $n_0 = 0.1$ the electrons energy is higher then in the case $n_0 = 10$, but lower for the ions energy. This can be explained considering that for $n_0 = 0.1$ the electrons energy is gradually increasing, while in the $n_0 = 10$ case we have a spike of absorption due to reflections of the overdense plasma. This also means that in the $n_0 = 0.1$ case the energy transfer between electrons and ions will be slower, in fact the $n_0 = 0.1$ ions energy will be higher then $n_0 = 10$ only at $t \sim 350fs$, thus $100fs$ later then the electron population. This behaviour can be seen in the temperature estimates, at $300fs$: $T_{ele}(n_0 = 0.1) > T_{ele}(n_0 = 10)$, while $T_{ion}(n_0 = 0.1) < T_{ion}(n_0 = 10)$.

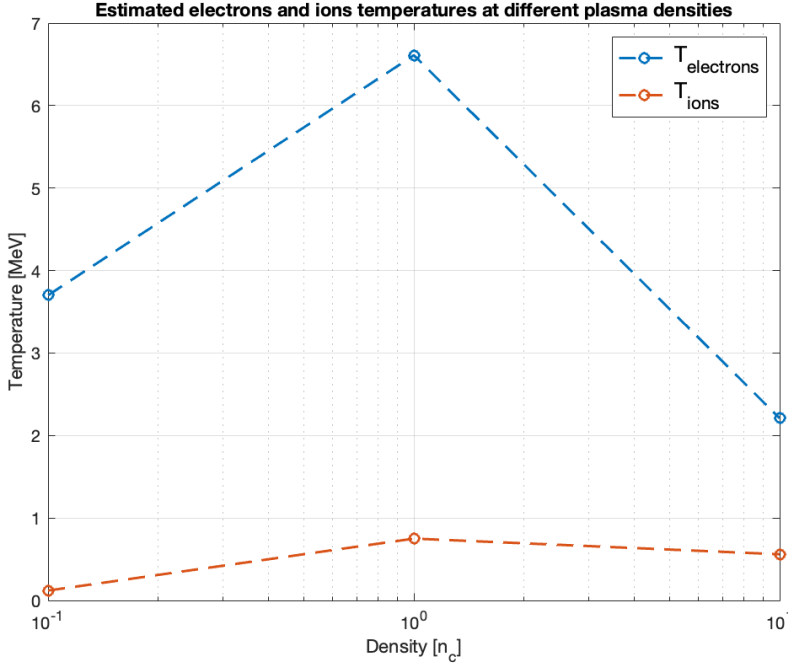


Figure 11: Plot of the electrons and ions temperatures for $a_0 = 10$, n_0 variable, at $t = 300 fs$.

4 Bonus task: TNSA

Energetic ions have a wide variety of applications. Their production is normally implemented through the use of accelerators, which require large facilities and large quantities of energy. The use of plasma allows a new kind of technology to be implemented for the production of these energetic ions, lowering both spatial and energetic requirements. Target Normal Sheath Acceleration (TNSA) exploits plasma laser interaction to transfer energy from an high energy laser beam to the electrons in a solid plasma target. The electrons will move, thus generating an electric field that will accelerate the ions. This approach allows the acceleration of ions in the order of tens of MeV per cm.

Recent development in the research led to the enhancement of a Double-Layer Target (DLT). The use of a thick coating layer of heavy ions (often Carbon) with a near critical density placed in front of the main target results in a more efficient acceleration of the light ions from the back of the foil. This has been attributed to several phenomena: the laser self-focusing (SF) induced by the radial dependence of the refractive index within the channel generated via the ponderomotive force, the generation of a strongly magnetized channel carrying high currents and the Direct Laser Acceleration of electrons (DLA) through the betatron resonance. [2]

A TNSA event hides quite convoluted physic's dynamics that complicate the process' optimization. DLT further hinders the tuning of the configuration due to the addition of the mechanism mentioned above.

We simulated a TNSA with a DLT configuration composed of a 1 um thick contaminant layer (electrons and carbon ions) as the main target with a second 15 nm thick layer (electrons and protons) on the rear side of the main target. Different stages of the simulation are shown in Figures 12 \div 14. A complete video of the simulation is available on Github.

A plot for the energies of the ions as a function of time has been provided in Figure 15. It can be noticed that Carbon ions gain energy earlier than protons, because of the spatial disposition in the target. Protons' energy quickly rises after a brief delay and near timestamp $150 fs$, they overcome Carbon's energy.

A plot for the temperature of the different species is also proposed. The temperature variation has been obtained through the fitting of the energy spectra as in Question 2. From this plot we can highlight the linear dependence of the protons' energy from the electron temperature: they reach their maximum value when the electrons reach their maximum temperature as well. From theory [2] we

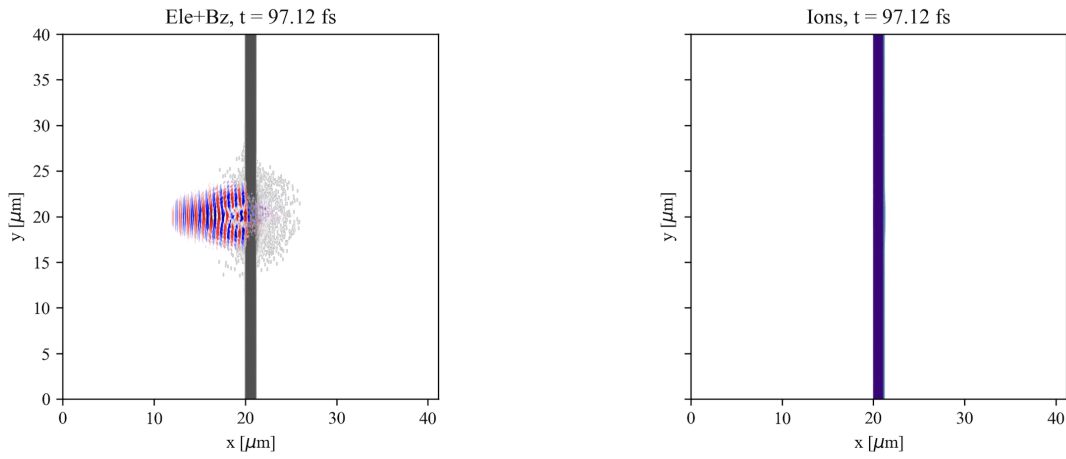


Figure 12: The laser is impinging the target, electrons are in motion while ions are still.

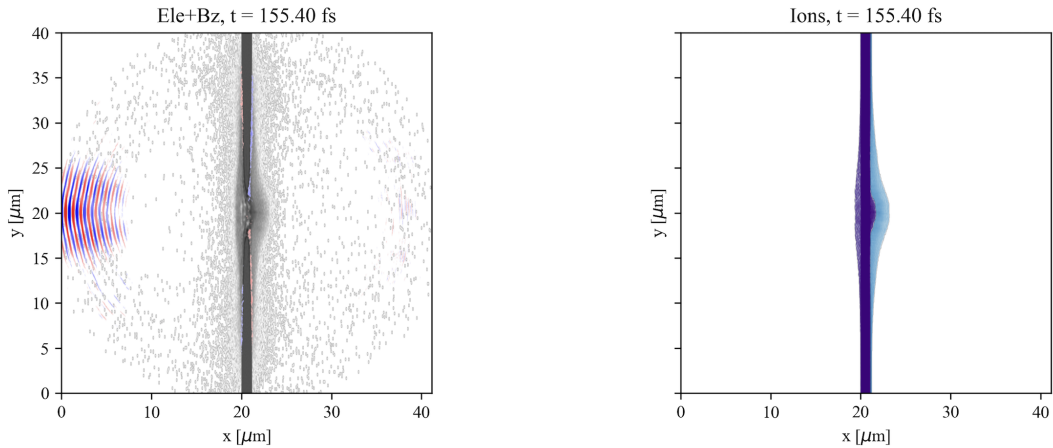


Figure 13: The laser has been reflected, electrons have formed an electric field sheath that is starting to move the ions.

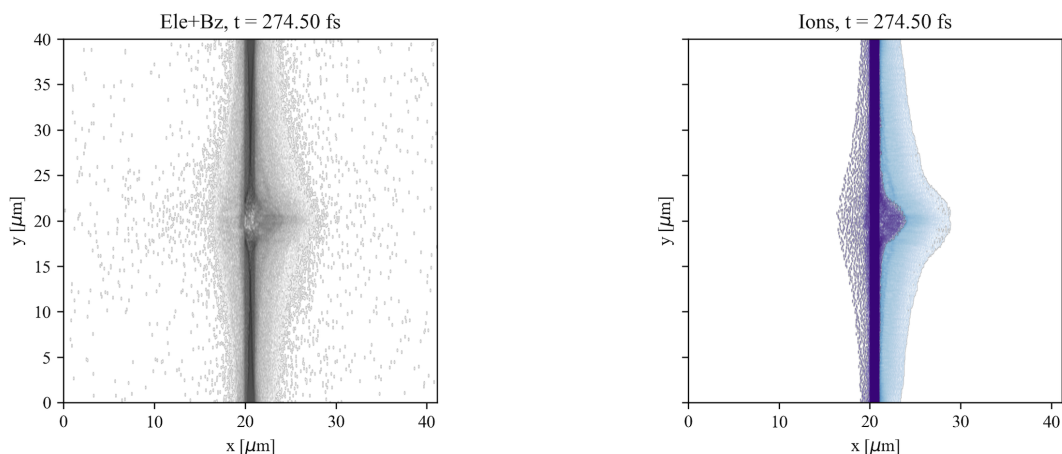


Figure 14: Ions are being accelerated, it is possible to notice the different magnitude of acceleration due to the different mass of Carbon (front of the target) and protons (back of the target). Video.

know that the maximum is at the self focusing focal length.

In Table 2 we tabulated the various specie temperatures at different timestamps. A final observation about electron temperature is due because their distribution is heavily non-Maxwellian, so the resulting temperature is heavily influenced by the point of the distribution we choose to interpolate.

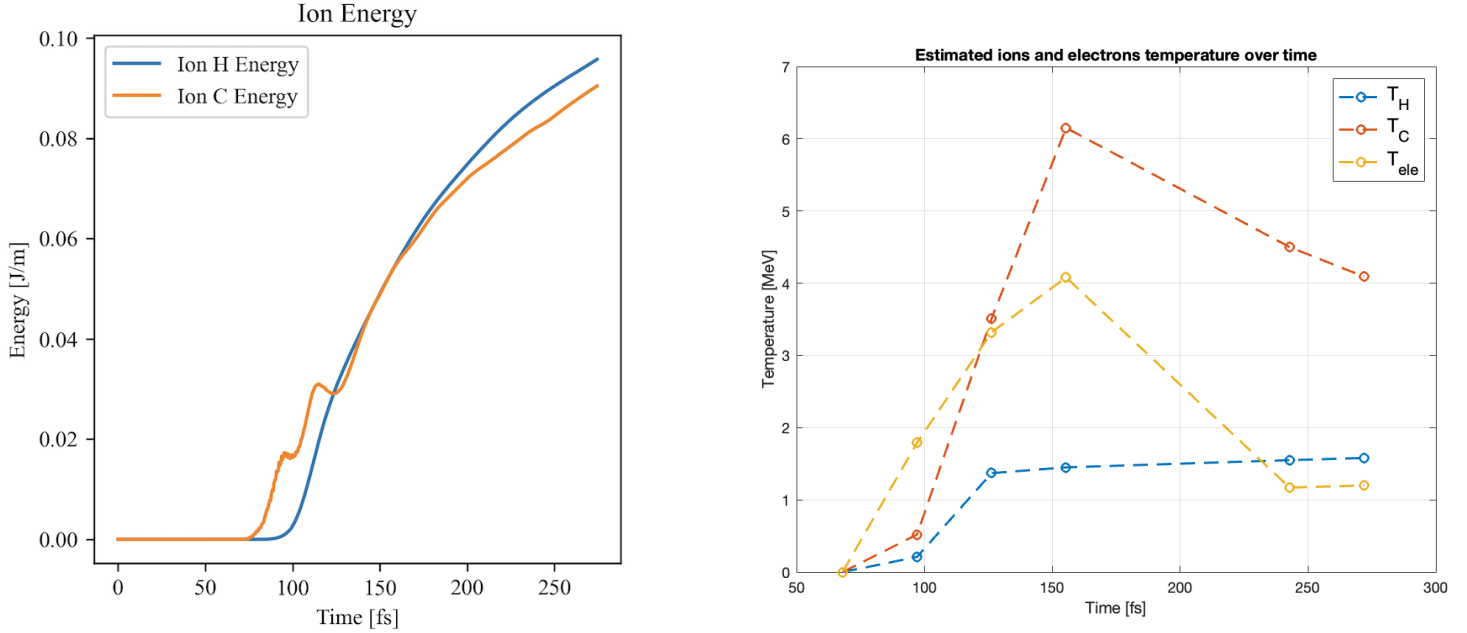


Figure 15: Ions energy and species temperature as a function of time.

t [fs]	T_{ele} [MeV]	T_H [MeV]	T_C [MeV]
67.99	~ 0	~ 0	~ 0
97.12	1.79	0.21	0.52
126.26	~ 3.32	1.37	3.51
155.40	~ 4.08	1.45	6.15
242.81	1.17	1.55	4.50
271.95	1.20	1.58	4.09

Table 2: Species temperature at different timestamps.

References

- [1] Github repository: https://github.com/glecce3/plasma_computational_lab2_results
- [2] A. Pazzaglia, L. Fedeli, A. Formenti, A. Maffini, and M. Passoni, "A theoretical model of laser-driven ion acceleration from near-critical double-layer targets," *Commun Phys*, vol. 3, no. 1, p. 133, Aug. 2020, doi: 10.1038/s42005-020-00400-7.
- [3] L. Fedeli, A. Formenti, C. E. Bottani, and M. Passoni, "Parametric investigation of laser interaction with uniform and nanostructured near-critical plasmas," *Eur. Phys. J. D*, vol. 71, no. 8, p. 202, Aug. 2017, doi: 10.1140/epjd/e2017-80222-7.
- [4] P. K. Tiwari, R. Kumar, K. Halder, and Y. S. Lee, "Maxwell–Boltzmann and Druyvesteyn Distribution Functions Expressing the Particle Velocity and the Energy in Sheath Plasmas," *J Russ Laser Res*, vol. 44, no. 5, pp. 504–512, Sep. 2023, doi: 10.1007/s10946-023-10157-3.
- [5] Robert Babjak, Bertrand Martinez, Miroslav Krus, Marija Vranic "Direct laser acceleration in varying plasma density profiles" <https://doi.org/10.48550/arXiv.2406.10702>